

Onset of Irreversibility in Cyclic Shear of Granular Packings

Steven Slotterback¹, Mitch Mailman¹, Krisztian Ronaszegi¹,

Martin van Hecke², Michelle Girvan¹, and Wolfgang Losert^{1*}

¹*Department of Physics, and IREAP, University of Maryland, College Park, Maryland, 20742 and*

²*Kamerlingh Onnes Laboratory, Universiteit Leiden, PObox 9504, 2300RA Leiden, the Netherlands*

(Dated: September 26, 2011)

We investigate the onset of irreversibility in a dense granular medium subjected to cyclic shear in a split-bottom geometry. To probe the micro and mesoscale we image bead trajectories in 3D throughout a series of shear strain oscillations. Though beads lose and regain contact with neighbors during a cycle, the topology of the contact network exhibits reversible properties for small oscillation amplitudes. With increasing reversal amplitude a transition to an irreversible diffusive regime occurs.

PACS numbers: 81.05.Rm,45.70.-n,82.70.Kj,47.57.Gc,83.80.Fg

The transition from reversible to irreversible dynamics in systems of many interacting particles is of fundamental importance to many-body physics. Granular materials under repeated shear deformations constitute excellent experimental systems with which to study such reversibility for out-of-equilibrium systems. Since particles are macroscopic in size, the lack of thermal fluctuations [1] allows, at least in principle, for reversible particle trajectories. In ground breaking work on low concentration granular suspensions, Corté and coworkers observed that particle collisions tend to disrupt the inherent reversibility of low Reynolds number fluid flow, and that reversibility is lost at strains and densities that allow a particle to collide with two or more neighbors [2]. As a consequence, the onset of irreversibility decreases approximately as the square of particle density.

For dense particle systems close to jamming, the threshold for exact reversibility would thus become extremely small. However, dense configurations of particles have additional constraints on their positions: the cage formed by neighbors in the local environment of the particle confine its position, providing a new reference for the motion of the particle. Under shear strain, neighbors are lost, and correlations are important: rearrangements in dense configurations are highly collective and are known to exhibit local reversibility [3] as well as larger scale dynamical heterogeneities [4–6]. Under cyclic shear strain of such dense systems, the question thus becomes under what conditions, even in the absence of exact reversibility, neighbors reunite after one strain cycle.

In this Letter, we describe experiments which probe the full three dimensional motion of beads within a split-bottom shear cell undergoing cyclic shear. Dense granular systems under cyclic shear in two and three dimensions have been studied previously [4, 7–10], but the trajectories of all beads in the bulk have not been probed, and collective bead dynamics and reversibility are not well understood. Here we will determine under which conditions beads revert back to their original neighbors when shear flow is reversed, i.e., reversibility of the neighbor topology.

We find that Mean Square Displacements (MSD) of beads indicate a crossover between reversibility and irreversibility of the packing under cyclic shear, and a characteristic strain amplitude is associated with this crossover. The reversibility of neighbor changing events is analyzed through the use of the Broken Link Network [11], which assigns a link to pairs of particles in a reference then move apart, under shear strain. For small amplitudes, the number of broken links per cycle decreases with increasing cycle number, while for larger amplitudes the number of broken links is constant, and, collectively, broken links form clusters that involve a significant fraction of the system.

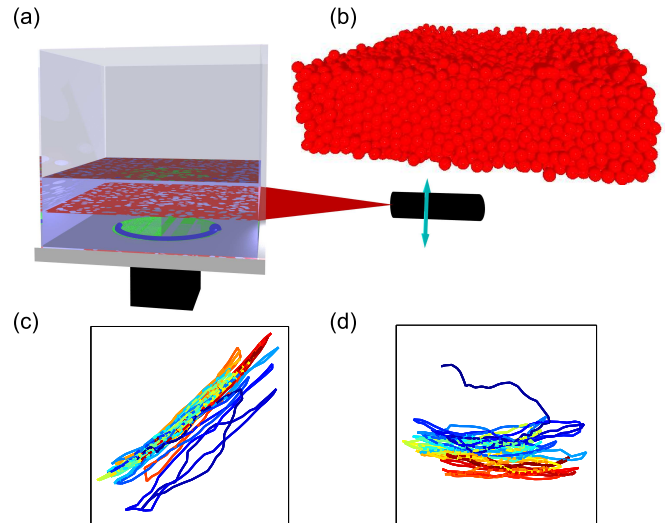


FIG. 1: (a) Split-bottom shear cell with acrylic beads in index matched, dyed fluid. A laser sheet pair illuminates a cross-sections for imaging. (b) As shown in this reconstruction, the position of all beads is found by scanning the laser sheet sheet across the whole container and automatic particle recognition. (c)-(d) A typical trajectory of a bead under oscillatory shear strain with a reversal amplitude of 40° from (c) above and (d) the side (cube sides are 2 bead diameters, color changes from blue to red color with increasing time).

Setup — To study motion of all beads, we built a modified version of the split-bottom geometry [12, 13] that allows for 3D imaging. In this geometry, shear is applied from below by rotating a disk mounted flush with the bottom. A shear zone is then emanating from the edge of a rotating disk — much of the shear zone is far from boundaries, the shear zone is wide and smooth, and nothing obstructs its view, making it ideally suited for 3D observations of grain flows with smooth gradients.

We use a square box with a 15 cm by 15 cm bottom and a 9 cm diameter disk at the bottom. In order to provide traction for the beads above, we attach a sparse coating of 3 mm beads to the bottom of the container and disk surface. We fill the container with 5 mm diameter acrylic beads to a height of 4.5 cm (9 bead diameters). We immerse the beads in an index matched fluid (Triton X-100). A fluorescent dye (Nile Blue 690 Perchlorate) is added to the fluid, along with a small amount of HCl (1.0 mL per 1.0 L of fluid) to stabilize the mixture.

We use the 3D imaging technique described in [14] and illustrated in Fig. 1, but with an improved bead finding algorithm. We use a 3D version of the convolution described in [15] to find the position of each bead to better than half a pixel, or 4% of a bead diameter. We then track the motion of individual beads with a tracking algorithm developed by Grier et al. [16] to find trajectories such as the one in Fig. 1c-d. With the full trajectories for about 98% of beads in our system outside the bottom layer, we can now analyze how beads move with respect to their neighbors.

On average, beads move with the disk near the disk, and stay stationary near the walls. We restrict our analysis to the wide shear zone which separates these regions. Specifically, for several axial sections, we calculate mean angular displacement as a function of radial displacement from the disk center over the time intervals preceding the first reversal event. For each section, we consider the annular region whose differential strain is within 40% of the maximum differential strain in that section. Thus, we exclude beads which are either moving too slow or are highly correlated with their neighbors. We have verified that our results are not particularly sensitive to the details of shear zone extraction.

Imaging cannot distinguish whether two hard spheres are in contact or just close together; instead we choose a maximum separation criterion to identify the nearest neighbors of each bead based on a preference for tangential motion of neighboring beads [11, 17]. Based on this criterion, we consider beads whose centers are within ≈ 1.08 bead diameters of one another to be nearest neighbors, since beads that are separated by greater distances show no such preference for tangential relative motion. Thus, the beads have an effective radius $R = 0.54$ bead diameters.

Protocol — To create reproducible initial conditions representative of steady shear, we rotate the disk two

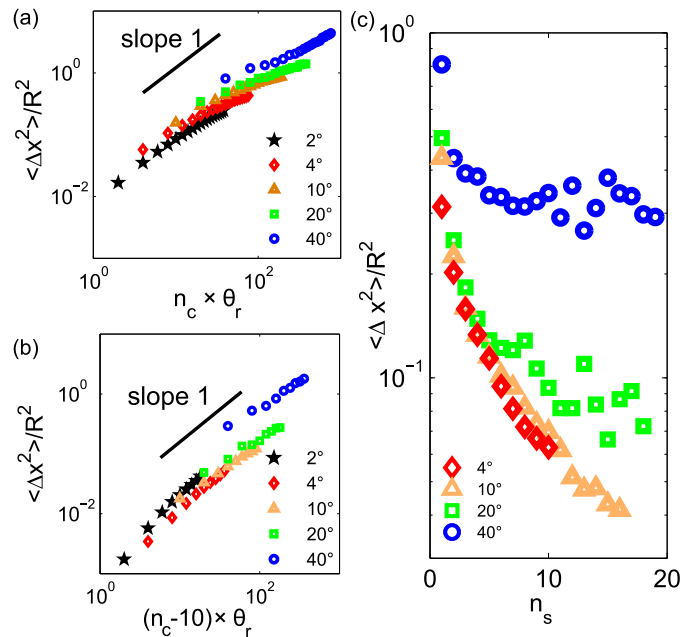


FIG. 2: (a)-(b) Mean Square Displacements (MSDs) at the end of each cycle as a function of cycle number for different cycle amplitudes, scaled by the effective bead radius R : (a) Reference frame at the start of the first cycle, (b) The start of the 10th cycle is chosen as a reference frame. (c) MSD after 80° of absolute strain vs. reference cycle number.

full revolutions at 1 mrad/sec. At this rate of strain, the granular flow in our fluid immersed system is independent of strain rate, with the same velocity profile as a dry granular flow [18]. We then reverse the direction of rotation of the disk and move the disk for a strain of θ_r ($= 2^\circ, 4^\circ, 10^\circ, 20^\circ, 40^\circ$). We reverse the direction again and rotate the disk by $-\theta_r$ to its original position, thus straining and reversing the system in a cyclic fashion. We perform 20 successive cycles in each experiment, taking a 3D image of the system after every 2° of strain.

Mean Square Displacements — The first measure of reversibility we employ is to test how far a bead has moved after a full cycle. The mean square displacements (MSD) of the beads in the shear zone at the end of each of the 20 cycles are shown as function of cycle number, n_c , in Fig. 2a. For all but the largest reversal amplitude θ_r , the slope of the MSD decreases with increasing cycle number signalling sub-diffusive behavior.

To explore whether the system becomes more reversible after several shear cycles, we choose the beginning frame of a later starting cycle n_s as a reference frame. Fig. 2b illustrates that for $n_s = 10$, the MSD is up to an order of magnitude smaller, suggesting that bead positions in this cyclic shear flow become more reversible after several cycles. Strikingly, the MSD for the largest reversal amplitude ($\theta_r = 40^\circ$) is considerably larger in magnitude.

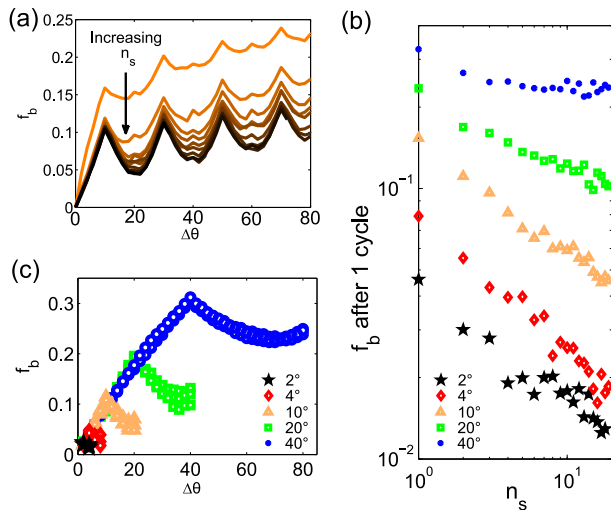


FIG. 3: (a) Fraction of links broken, f_b for shear reversal vs. 2° strain step for the case of $\theta_r = 10^\circ$. (b) f_b after one cycle as a function of the starting cycle n_s , for all θ_r . (c) f_b as a function of $\Delta\theta$ for representative curves at $n_s=5, 10$ and 15 .

To compare the rearrangements after one cycle of amplitude θ_r with two cycles of amplitude $\theta_r/2$ etc, we calculate the MSD after a fixed absolute strain $\Delta\theta$ (relative to a chosen reference frame) which we fix here at 80° . Fig. 2c shows the MSD at this fixed total strain as function of the start cycle n_s . We see that for $\theta_r = 40^\circ$, the magnitude of the MSD does not depend strongly on the choice of reference cycle after a short transient of about 3 cycles, while the MSD for smaller θ_r continue a downward trend for all cycles investigated.

All three probes of the MSD strongly suggest a qualitative change in behavior between $\theta_r = 20^\circ$ and $\theta_r = 40^\circ$: for large amplitude, the motion is irreversible, and reaches a steady, diffusive state, while for small amplitudes, the cyclic shear strain process becomes increasingly reversible and the system is aging.

Broken Links — As a second measure of reversibility we probe the network of nearest neighbors. We first identify all neighbors in a reference frame at the start of a cycle. Then we calculate, as function of frame number, the fraction of links broken f_b , defined as the fraction of neighbor pairs from the reference frame that are no longer within the cutoff distance used to define neighbors. The approach of [11] has been modified here to include the possibility of “healing,” which is the removal of a broken link when a neighbor pair from the reference frame reforms after being broken in an intermediate frame. Note that other pairs of beads may become neighbors in later frames but this is not considered in the broken link analysis.

In Fig. 3a we show the evolution of f_b as a function of $\Delta\theta$, for $\theta_r = 10^\circ$ — other θ_r show comparable results. The top curve shows f_b with $n_s=1$. We observe a strong

decrease in f_b when the strain direction is reversed (at 10°) — broken links reform after reversal. Additionally, fewer additional links are broken in each subsequent cycle — the motion becomes less irreversible for later times. The ten lower curves in Fig. 3a show f_b when the start of a later cycle is chosen as a reference frame, illustrating that the recovery of neighbors after a full shear strain cycle (at arrow) improves with increasing cycle number.

In Fig. 3b we show f_b after one cycle as a function of the starting cycle n_s , which provides a local measure of the reversibility of the configuration after one cycle. Clearly, the fraction of links broken decreases with increasing n_s (indicating an increase in reversibility) for all but the largest reversal amplitude, which appears to level off. As a simple local metric, f_b captures what fraction of the neighbor network is evolving with strain, a topological analog to the “particle activity” of [2]. Indeed, the apparent power dependence of the decay on n_s in the reversible regime, and a leveling off for the highest reversal amplitude, is consistent with the observation of a reversible-irreversible transition observed in [2]. However, as illustrated in Fig. 3c, f_b cannot identify this local reversibility in the neighbor network over the period of one cycle - f_b after one cycle increases approximately linearly with cycle amplitude without a clear change in the form of the dependence on $\Delta\theta$.

Our characterization of the irreversibility revealed a striking difference between the growth of mean square displacements and fraction of links broken with driving amplitude θ_r . The MSD barely grows with θ_r for small driving amplitudes (see in particular Fig. 2c for small start cycles, where all data for θ_r from 4° to 20° strongly overlap), but then exhibits a jump for $\theta_r = 40^\circ$. In contrast, the fraction of links broken f_b grows approximately linearly with θ_r (see Fig. 3c) and so over a single strain cycle f_b fails to distinguish $\theta_r = 40$ from the smaller reversal amplitudes.

We believe that this difference occurs along with the percolation of the network of links broken. In this picture, a small fraction of links broken leads to small clusters of failures that upon reversal are mostly healed. Consequently, after a cycle the beads return to their starting position, leading to a small MSD. However, once the fraction of links broken is sufficiently large, a dominant failing cluster forms. Upon reversal, this dominant failing cluster is not fully healed, and after one cycle, beads end up with different neighbors and at different locations, leading to a large MSD.

To probe this picture, we investigate how links that break are connected with each other, i.e., the topology of the broken links network. Under steady shear, it is known that the size of the largest component, i.e., the largest cluster of beads exhibiting inter-connected broken links, shows a transition beyond a characteristic strain (see [11]). Here we adopt this measure to oscillatory shear strain, and follow s_g , which is the fraction of beads in

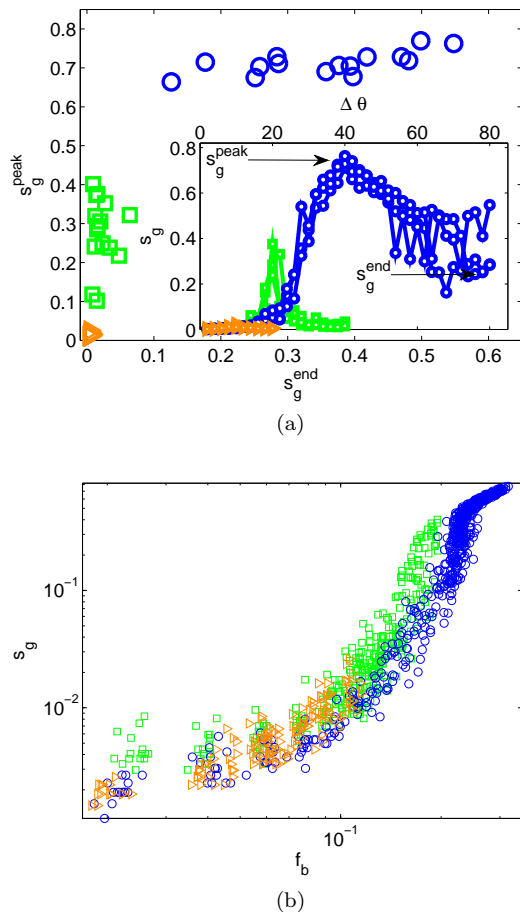


FIG. 4: (a) The peak largest component size versus the final largest component size, for each cycle. (a, Inset) s_g as a function of $\Delta\theta$ over one cycle for $n_s = 5, 10,$ and 15 . Peak and end values for s_g are pointed to for the 40° case. (b) s_g as a function of the fraction of links broken f_b for each reference network used, for reversal amplitudes of 10° (orange triangles), 20° (green squares) and 40° (blue circles).

the largest component, as function of absolute strain $\Delta\theta$, with reference frames chosen at the beginning of each cycle.

Fig. 4 provides qualitative support for our picture. In the inset of Fig. 4a we show that for $\theta_r \leq 20^\circ$, the size of the largest component s_g initially grows with $\Delta\theta$ but then shrinks back to almost zero when the motion is reversed (links are reformed after reversal), while for $\theta_r = 40^\circ$, s_g remains substantial after completing a full cycle — hence links remain broken. To stress this qualitative difference, we collect the data for the last 15 cycles, characterize the functional form of $s_g(\Delta\theta)$ by its peak size at the reversal, s_g^{peak} , and the largest component size at the end of the cycle, s_g^{end} , and make a scatter plot of s_g^{peak} versus s_g^{end} (Fig. 4a). This reveals a clear separation of the 10° and 20° data which form peak component sizes that can be almost fully reduced to zero, from the largest amplitude

40° where broken links interconnect a significant part of the system at the end of a cycle.

In Fig. 4b we show scatter plots of s_g versus f_b for three cycle amplitudes, which show that for each cycle amplitude, the data collapses onto a master curve quantitatively similar to that of [11]. For the largest driving amplitude, a regime emerges where s_g has a dependence on f_b that is consistent with a power law — a collective, percolation effect.

Discussion — We have studied a granular system under shear reversal at microscopic and mesoscopic scales. Such dense systems are never strictly reversible, but we have shown that irreversibility comes in two distinct flavors. For small driving amplitudes, neighbor links are broken but most reform, there are no large clusters, and the mean square displacements are small, and importantly, the cycle-to-cycle mean square displacements decrease with cycle number: the system is aging. However, for large driving amplitudes, a substantial fraction of neighbor links do not reform upon reversal, and the cycle-to-cycle mean square displacements become independent of cycle number: here the motion becomes diffusive. Our data is consistent with the hypothesis that this strong irreversibility at large cycle amplitudes is connected to the growth of a giant component, which signifies a collective breaking of contacts involving a number of beads that is proportional to the system size. We further showed that the growth of the largest component is consistent with a power law dependence on f_b for the largest reversal amplitude.

We note that our new topological measures of irreversibility — though less stringent than exact reversal symmetry of the equations of motion — correlate well with a strong increase in MSD with cycle amplitude (Fig. 2c), and thus are likely relevant for important granular materials properties such as mixing and segregation.

One important future direction of study will be to connect the onset of irreversibility in bead configuration to the emergence of dynamical heterogeneities. It is important to note that this work has probed in detail time scales much shorter than those at which dynamical heterogeneities are observed in, for instance, [6]. As a result, our observations are likely related to the formation of the building blocks of dynamical heterogeneities, whose dynamics may unfold at much larger time scales.

We thank Joost Weijs for his contributions to our particle extraction routine, William Derek Updegraff for his assistance in experimentation, as well as Mark Herrera for his assistance in analysis. This work was supported by NSF grant DMR0907146. KR was supported by the Rosztoczy Foundation.

* Electronic address: wlosert@umd.edu

- [1] J. Duran, *Sands, Powders, and Grains* (Springer, New York, 2000).
- [2] L. Corté, P. M. Chaikin, et al., *Nature Physics* **4**, 420 (2008).
- [3] M. Lundberg, K. Krishan, et al., *Phys. Rev. E* **77**, 041505 (2008).
- [4] O. Dauchot, G. Marty, et al., *Phys. Rev. Lett.* **95**, 265701 (2005).
- [5] G. Marty and O. Dauchot, *Phys. Rev. Lett.* **94**, 015701 (2005).
- [6] R. Candelier, O. Dauchot, et al., *Phys. Rev. Lett.* **102**, 088001 (2009).
- [7] A. Panaitescu and A. Kudrolli, *Phys. Rev. E* **81**, 060301 (2010).
- [8] J. Zhang, J. Ren, et al., *AIP Conference Proceedings* **1145**, 553 (2009).
- [9] M. Toiya, J. Stambaugh, et al., *Phys. Rev. Lett.* **93**, 088001 (2004).
- [10] N. W. Mueggenburg, *Phys. Rev. E* **71**, 031301 (2005).
- [11] M. Herrera, S. McCarthy, et al., *Phys. Rev. E* **83**, 061303 (2011).
- [12] D. Fenistein, J. W. van de Meent, et al., *Phys. Rev. Lett.* **92**, 094301 (2004).
- [13] D. Fenistein and M. van Hecke, *Nature* **425**, 256 (2003).
- [14] S. Slotterback, M. Toiya, et al., *Phys. Rev. Lett.* **101**, 258001 (2008).
- [15] J.-C. Tsai and J. P. Gollub, *Phys. Rev. E* **70**, 031303 (2004).
- [16] J. Crocker and D. Grier, *J. Colloid Interface Sci.* **179**, 298 (1996).
- [17] S. Slotterback, L. Goff, et al., *AIP Conference Proceedings* **1145**, 489 (2009).
- [18] J. A. Dijksman, E. Wandersman, et al., *Phys. Rev. E* **82**, 060301 (2010).